

A Differential Approach for Gaze Estimation

Gang Liu, Yu Yu, Kenneth A. Funes Mora, Jean-Marc Odobez*

arXiv:1904.09459v1 [cs.CV] 20 Apr 2019

Abstract—Non-invasive gaze estimation methods usually regress gaze directions directly from a single face or eye image. However, due to important variabilities in eye shapes and inner eye structures amongst individuals, universal models obtain limited accuracies and their output usually exhibit high variance as well as biases which are subject dependent. Therefore, increasing accuracy is usually done through calibration, allowing gaze predictions for a subject to be mapped to his/her actual gaze. In this paper, we introduce a novel image differential method for gaze estimation. We propose to directly train a differential convolutional neural network to predict the gaze differences between two eye input images of the same subject. Then, given a set of subject specific calibration images, we can use the inferred differences to predict the gaze direction of a novel eye sample. The assumption is that by allowing the comparison between two eye images, annoyance factors (alignment, eyelid closing, illumination perturbations) which usually plague single image prediction methods can be much reduced, allowing better prediction altogether. Experiments on 3 public datasets validate our approach which constantly outperforms state-of-the-art methods even when using only one calibration sample or when the latter methods are followed by subject specific gaze adaptation.

I. INTRODUCTION

Gaze is an important cue of human behaviours. Gaze directions and gaze changing behaviours (such as gaze aversion, the intentional redirection away from the face of interlocutor [1]) are good indicators of the visual attention and are also related to internal thoughts or mental states of people. Besides, as a non-verbal behaviour, gaze is an important communication cue which has also been shown to be related to higher-level characteristics such as personality. It thus finds applications in many domains like Human-Robot-Interaction (HRI) [1], [2], Virtual Reality [3], social interaction analysis [4], or health care [5], or mobile phone scenarios [6]–[8].

Motivation. Non-invasive vision based gaze estimation has been addressed with two main paradigms: geometric models and appearance [9]. Since the former suffers from noise, image resolution, illumination, or head pose issues, appearance-based methods which predict gaze directly from the eye (or face) images have attracted more attentions in recent years [10]–[13]. Among them, deep neural networks (DNN) have been shown to work well.

Nevertheless, even when using DNN regressors, their accuracy has been limited to around 5 to 6 degrees, with a high inter person variance [10]–[16]. This is due to many factors including dependencies on head poses, large eye shape variabilities, and only very subtle eye appearance changes when looking at targets separated by such small angle differences.

Gang Liu, Yu Yu, Jean-Marc Odobez are with the Idiap Research Institute, CH-1920, Martigny, Switzerland. E-mail: {gang.liu, yyu, odobez}@idiap.ch. Jean-Marc Odobez is the corresponding author.

Kenneth Alberto Funes Mora is with Eyeware Tech SA, CH-1920, Martigny, Switzerland. E-mail: kenneth@eyeware.ch.

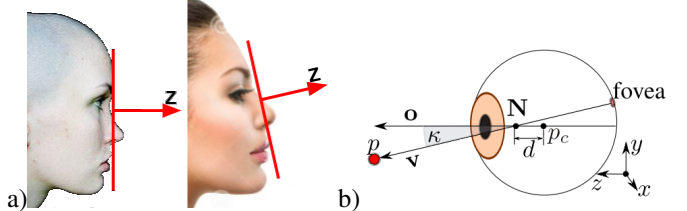


Fig. 1: Examples of variability factors. (a) Head pose shape variabilities induce different frontal head pose definition and hence variabilities in eye images. (images from Pinterest.com). (b) Variabilities across subjects of the difference between the visual axis (unobserved, defining gaze) and the optical axis (defined by iris centre, observed) introduces gaze prediction uncertainties (image from [18]).

For instance, Fig. 1(a) shows the difficulty to define an absolute head pose like a frontal pose. This has a non negligible impact on the eye appearance. Another factor explaining the limited accuracy when building person independent models is that the visual axis is not aligned with the optical axis (related to the observed iris) [17], and that such alignment differences are subject specific (see Fig. 1(b)), with a standard deviation of 2 to 3 degrees amongst the population without eye problems. Said differently, in theory, images of two eyes with the same appearance but with different internal eyeball structure can correspond to different gaze directions, demonstrating that gaze can not be fully predicted from the visual appearance. Altogether, in practice, such variabilities introduce confusions for regression, as illustrated in Fig. 2 which shows that gaze related elements (like iris location or the eyelid closing) in eye images from different persons sharing the same gaze directions can look quite different, while more importantly, eye of different persons can be similar when they look at different directions (see (a-2) and (d-3)).

A straightforward solution to this problem is to learn person-specific models [10], [19], [20] or fine-tune a pre-trained model [21]. Note that even regular high-end Infra-Red (IR) devices (eg from Tobii) require users to stare at several fixed positions before using them. However, training person-specific appearance models may require large amounts of personal data, especially for DNN methods and even when conducting simple network fine tuning adaptation. Other methods rely on fewer reference samples to train a linear regression model [22] or an SVR [6]. Still these methods are usually not robust to environment changes and their accuracy is heavily affected by the number of reference samples. A too small amount can even result in worse performance than without calibration. This is unfortunate, as there are plenty of real scenarios in which we can collect a few annotated samples.

Contributions. This paper is an extension of our paper [24]. we aim to solve the person-specific bias using a few annotated reference samples from the specific person. To this end, two

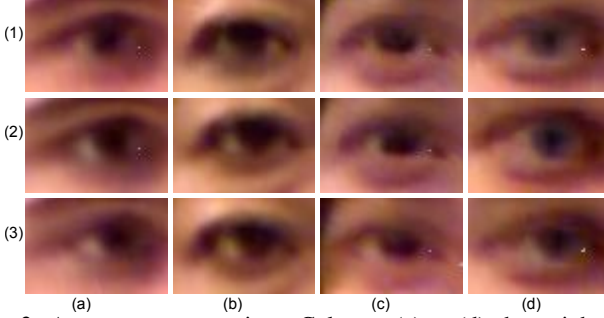


Fig. 2: Appearance comparison. Columns (a) to (d) show right eye images from different persons from the EYEDIAP dataset [23]. Row (1) to (3) correspond to gaze directions with the same pitch (5 degrees) and a yaw of 5, 10, 15 degrees respectively.

strategies have been proposed and analysed. The first one is a simpler method than those mentioned above for adaptation. It consists of learning the linear relationship between the gaze predictions from a pre-trained NN applied to few training samples and their groundtruth gaze, and is shown to achieve better results than the state-of-the art SVR method of [6].

Secondly, although the previous methods can reduce the subject specific bias between the subject (test) data and the overall training dataset, it does this by only working with the gaze prediction or feature outputs, and does not account for the high gaze prediction variance within each subject's data. To address this issue, our main contribution is to propose a differential gaze estimation approach, by training a differential NN to predict the gaze difference between two eye images instead of predicting the gaze directly. We hypothesize such a differential approach is less problematic than predicting gaze because the person dependent error (such as shape, alignment errors) will be alleviated. This is illustrated in Fig. 2, which shows that given an eye of a person, it is easier to judge whether it is looking more to the left or the right than a second eye image if the latter come from the same person than if it comes from another person (even with a similar eye shape). In Fig. 2, it is easier to see that the eye images at the bottom look more to the right than the eye images at top which are in the same column than compared to images in the other columns.

Our framework is illustrated in Fig. 3. At training time, a unified and person independent differential gaze prediction model is built which can be used at test time for person specific gaze inference relying on only a few calibration samples.

Thirdly, as there are many architectures that can be designed for differential gaze (early fusion by concatenating the two images, or fusion of feature maps of the two images at different levels), we investigate and compare different architectures and show that mid-level fusion is better than early fusion or late fusion. Usually they have different impacts on gaze estimation.

Paper organization. We discuss related works in Section II. In Section III, we introduce a state-of-the-art NN for gaze prediction, illustrate the subject specific bias problem, and propose a linear adaptation method to build subject specific gaze prediction models. In Section IV, we introduce our approach and the proposed modified siamese NN for differential gaze prediction. Experiments are presented in Section V, while Section VI concludes the work.

II. RELATED WORKS

Our work relates to appearance-based modelling, person dependent calibration methods, and to some extend, to siamese network approaches for achieving other tasks.

A. Appearance-based gaze estimation

As said earlier, geometric approaches rely on eye feature extraction (like glints when working with infrared systems, eye corners or iris centre localization) to learn a geometric model of the eye and then infer gaze direction using these features [25]–[30]. However, they usually require high resolution eye images for robust and accurate feature extraction, are prone to noise or illumination perturbations, and do not handle well head pose variabilities.

Hence, many recent methods rely on an appearance based paradigm [10]–[13] allowing them to be robust when dealing with low to mid-resolution images and to obtain good generalization performance. There, Neural networks (NN) methods have been shown to work well due to their ability to leverage large amount of data to train a regression network capturing the essential features of the eye images under various conditions like illumination and self-shadow, glasses, impact of head pose. For instance, [10] relied on a simple LeNet shallow network applied to eye images and first demonstrated that NNs outperform most other methods. Very recently, a deeper pretrained network (VGG-16 [31]) was fine-tuned for gaze estimation and further improved the accuracy [32]. In other directions, Kafka *et. al* [6] proposed to combine eye and face together using a multi-channel network, Zhang *et. al* [15] trained a weighted network to predict gaze from a full face image. Shrivastava *et. al* [14] learned a model from simulated eye images using a generative adversarial network.

B. Person dependent calibration

As explained in the introduction, person dependent calibration is critical to obtain a more robust and accurate model for gaze estimation (note that this is even the case for infrared head mounted device [33]–[35]). To solve this problem, Lu *et.al* [22] proposed an adaptive linear regression method relying on few training samples, but the eye representation (multi-grid normalized mean eye image) is not robust to environmental changes. Starting from a trained NN, Kafka *et.al.* [6] relied on eye images when looking at a grid of 13 dot sample. Feature maps from the last layer of the pretrained NN were then employed to train a Support-Vector-Regression (SVR) person specific gaze prediction model. However, SVR regression from a high dimensional feature vector input is not robust to noise. Different from [6], Masko tried to fine-tune the last layer of a pre-trained model for each subject, but this requires large amounts of data. In another direction, Zhang *et.al.* [36] proposed to train person-specific gaze estimators from user interactions with multiple devices, such as mobile phone, tablet, laptop, or smart TVs, but this does not correspond to the majority of use cases.

However, none of the above works have proposed to calibrate gaze by estimating gaze difference from reference

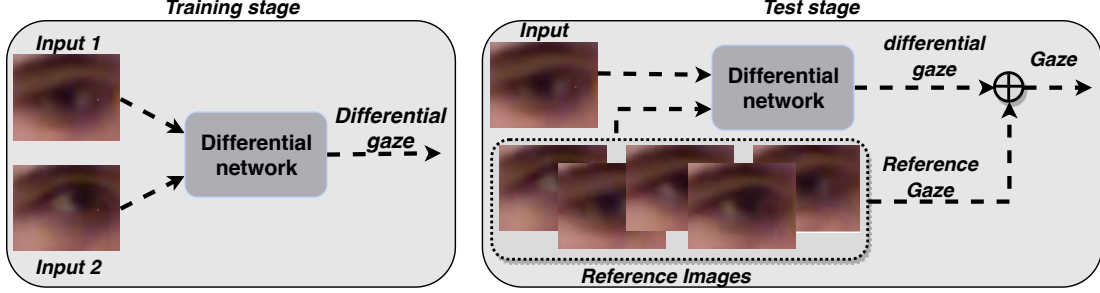


Fig. 3: Approach overview. During training, random pairs of samples from the same eye are used to train a siamese differential network. At test time, given a set of reference samples, gaze differences are computed and used to infer the gaze of the input image.

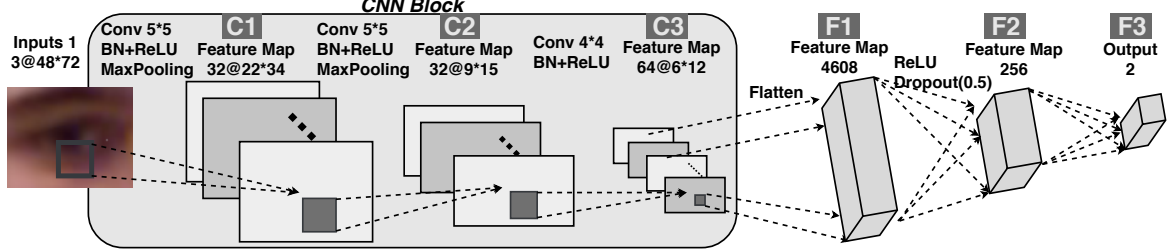


Fig. 4: Baseline CNN structure for gaze estimation.

images, which as we show in this paper is a much more robust approach requiring less reference images.

C. Siamese network

Siamese networks have first been proposed in [37] for signature verification. With the deep learning revival, they have been widely considered for tasks like feature extraction [38]–[40], image matching and retrieval [41], [42], person re-identification [43], [44]. They usually consist of two parallel networks with shared weights, in which a pair of distinct images is used as input, one for each network, and the distance between their outputs is taken as the siamese network output. Implicitly, when dealing with discrete category problems, the goal is to learn a mapping from the image space to a new feature space such that samples from the same class are close, while samples from different classes are far. In the regression case (our case), the loss function is usually defined by comparing the output distance with the groundtruth one.

The closest work to ours is Venturelli *et.al.* [45]. However, they are addressing a different task (head pose estimation), and their goal was more to use a multi-task approach in which both absolute head poses and head pose differences were used as loss function. At test time, the pose is still directly predicted from a single input image. Hence, while several layers of our differential networks are used to predict the gaze difference, in their case the pose differences was only computed from the network pose prediction output.

III. BASELINE CNN APPROACH AND LINEAR ADAPTATION

In this section, we first introduce a standard convolution neural network (CNN) for person independent gaze estimation. We then show the resulting bias existing for unknown individuals, and present our proposed linear adaptation method on how to solve it.

A. Gaze estimation with CNN

Network structure. Fig. 4 presents the standard NN structure for gaze estimation. It consists of three convolutional layers and two fully connected layers¹. More precisely, the input eye image $I \in \mathbb{R}^{M \times N \times C}$, where $(M, N, C) = (48, 72, 3)$ denote the dimensions and number of channels of the image, is first whitened. The convolutional layers are then applied and the resulting feature maps are flattened to be fed into the fully-connected layers. The predicted gaze direction $\mathbf{g}^p(I) \in \mathbb{R}^{2 \times 1}$ is regressed at the last layer. The details of the network parameters can be found in the figure.

Loss function. Denoting the gaze groundtruth of an eye image I by $\mathbf{g}^{gt}(I)$, we used the following L1 loss function:

$$\mathcal{L} = \frac{1}{|\mathcal{D}|} \sum_{I \in \mathcal{D}} \|\mathbf{g}^p(I) - \mathbf{g}^{gt}(I)\|_1, \quad (1)$$

where \mathcal{D} denotes the training dataset and $|\cdot|$ denotes the cardinality operator.

Network training. For eye images in the dataset, we first resize them into a fixed resolution $s = 48 \times 72$. Concretely, we upsample the images using bilinear interpolation if their sizes are smaller than s (MPIIGaze dataset). Otherwise, we randomly crop patches with size s around eyes (EYEDIAP dataset). The input has either three channels for color images as shown in Fig. 4, or one channel for gray scale images.

The network is optimized with Adam method, with a learning rate initially set to 0.001 and then divided by 2 after each epoch. In our experiment, 10 epochs are applied and proved to be sufficient. The mini batch size is 128.

B. Bias analysis and linear adaptation

Because each individual eye has specific characteristics (including internal non-visible dimensions or structures), in

¹Note that it is slightly different from [10].

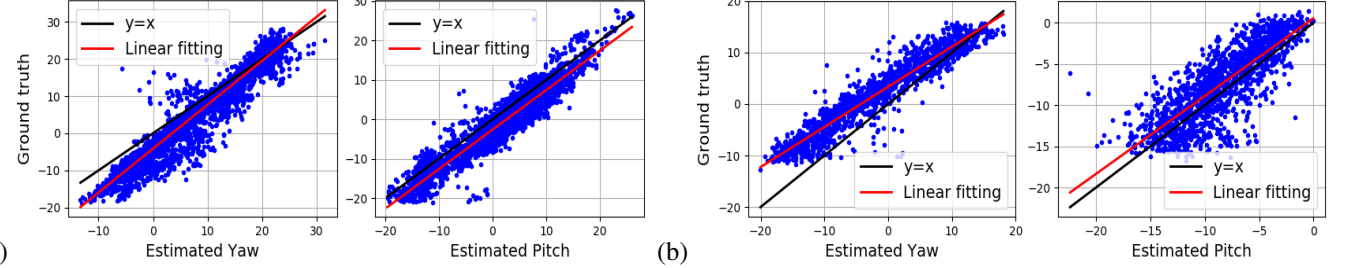


Fig. 5: Scatter plot of the network regression (X-axis) and labelled groundtruth (Y-axis) of the yaw (left plot) and pitch (right plot) angles for an individual eye taken in the (a) EYEDIAP dataset; and (b) MPIIGaze dataset.

practice, we often observe a data bias between the network regression $\mathbf{g}^p(I)$ and the labelled groundtruth $\mathbf{g}^{gt}(I)$ of the eye images $I \in \mathcal{D}_{Test}$ belonging to a single person. This is illustrated in Fig. 5, which provides a scatter plot of the $(\mathbf{g}^p(I), \mathbf{g}^{gt}(I))$ angle pairs in typical cases, which can be compared with the identity mapping (black lines).

As can be observed, there is usually a linear relationship between $\mathbf{g}^{gt}(I)$ and $\mathbf{g}^p(I)$, which is illustrated by the red lines in the plots. Thus, when a set \mathcal{D}_c of sample calibration points of a user (usually 9 to 25 points) is available, we propose to learn this relation and obtain an adapted gaze model \mathbf{g}^{ad} by fitting a linear model

$$\mathbf{g}^{ad}(I) = A \mathbf{g}^p(I) + B \quad (2)$$

where $A \in R^{2 \times 2}$ and $B \in R^{1 \times 2}$ are the linear parameters of the model which can be estimated through least mean square error (LMSE) optimisation using the calibration data.

IV. PROPOSED DIFFERENTIAL APPROACH

A. Approach overview.

The linear adaptation above allows to correct biases from the gaze output, but this does not really account for the specificity of a user's eye, nor was the network trained to take into account the presence of biases. The method we propose aims at solving these issues. It is illustrated in Fig. 3. Its main part is a differential network designed and trained to predict the differences in gaze direction between two images of the same eye. At test time, the gaze differences between the input eye image and a set of reference images are computed first. Then the gaze of the eye image is estimated by adding these gaze differences to the reference gazes. The details of the different components are introduced in the following paragraphs.

B. Differential network architecture.

The network we use is illustrated in Fig. 6, and is modified from the traditional siamese approach. Each branch in the parallel structure is composed of three convolutional neural layers, all of them followed by batch normalization and ReLU units. Max pooling is applied after the first and second layers for reducing the image dimensions. After the third layer, the feature maps of the two input images are flattened and concatenated into a new tensor. Then two fully-connected layers are applied on the tensor to predict the gaze difference between the two input images. Thus, where traditional siamese approaches would predict the gaze for each image, and compute the differences from these predictions, our approach uses neural

network layers to predict this difference from an intermediate eye feature representation.

The architecture we propose has several advantages. First, given the image input it seems to be a good compromise between prediction capacity and over-fitting. Secondly, while we could directly provide the two images as input to the network, this could increase the computational cost and not necessarily provide better prediction. We demonstrate this in the experimental section.

C. Loss function.

The differential network is trained using a set of random image pairs (I, J) coming from the same eye in the training data. Denoting by $\mathbf{d}^p(I, J)$ the gaze difference predicted by the network, we can define the loss function as:

$$\mathcal{L}_{diff} = \sum_{(I, J) \in \mathcal{D}^k \times \mathcal{D}^k} \|\mathbf{d}^p(I, J) - (\mathbf{g}^{gt}(I) - \mathbf{g}^{gt}(J))\|_1, \quad (3)$$

where \mathcal{D}^k is the subset of \mathcal{D} that only contains images of the same eye² of person k .

Network training. Optimization is done with the Adam method and an initial learning rate of 0.001 which is divided by 2 after each epoch. In experiments, 20 epochs are applied. The mini batch size is 128. To reduce the number of possible image pairs, we have constructed the dataset of pairs by using each image $I \in \mathcal{D}^k$ as first image and randomly selecting the second image J in \mathcal{D}^k .

D. Gaze inference at test time.

As the network predicts gaze differences only, the method requires at least one reference image to predict an absolute gaze vector. In practice, we rely on a small calibration set \mathcal{D}_c of images of the same eye. Thus, we predict the gaze difference $\mathbf{d}^p(I, F)$ between the test image I and the reference images F , and combine these gaze difference with the gaze groundtruth $\mathbf{g}^{gt}(F)$ to infer the gaze direction of the test image as $\mathbf{g}^{gt}(F) + \mathbf{d}^p(I, F)$. More formally:

$$\mathbf{g}^{sm}(I) = \frac{\sum_{F \in \mathcal{D}_c} w(\mathbf{d}^p(I, F)) \cdot (\mathbf{g}^{gt}(F) + \mathbf{d}^p(I, F))}{\sum_{F \in \mathcal{D}_c} w(\mathbf{d}^p(I, F))}, \quad (4)$$

where $w(\cdot)$ is weighting the importance of each prediction.

Intuitively, if the reference eye image is more similar to the test eye image, we should be more confident about the gaze

²Note: we learn separately a model for the left and the right eyes.

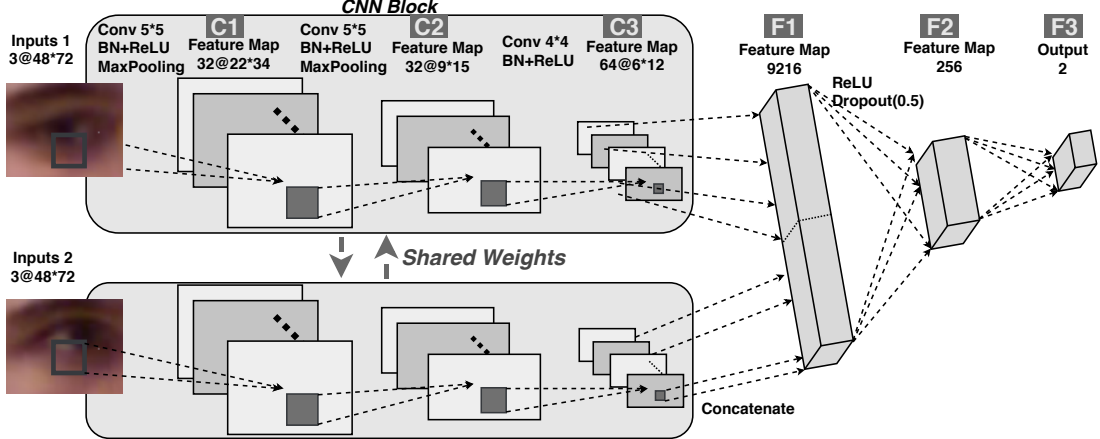


Fig. 6: The designed differential network for predicting gaze differences.

difference. Thus the weight has been defined as a function of $\mathbf{d}^p(I, F)$, which is a good indication of such similarity. In practice, we simply use a zero-mean Gaussian $\mathcal{N}(0, \sigma)$ as weight function. If σ is too small, reference samples with large gaze difference will have no contribution. While if σ is too large, reference samples will almost all have equal weights. In experiments, $\sigma = 5.7$ degrees proves to be a good choice on all test sets, and we discuss this in Section. V-E.

V. EXPERIMENTAL RESULTS AND ANALYSIS

In this section we thoroughly evaluate our algorithms and compare them with the-state-of-the-art methods on public datasets. In a second step, we discuss the impact of several important factors: choice and number of reference images, weighting scheme, architecture design, and model complexity.

A. Datasets

Since our method is designed for dealing with eye image alone, without extra information from the face, we considered the three following public eye-gaze datasets for validation.

EYEDIAP. This dataset contains 94 videos associated with 16 subjects [23]. Videos belong to three categories: continuous screen (CS) target, discrete screen (DS) target or floating target (FT). The CS videos were used in our experiments, which comprises static pose (SP) recordings where subjects approximately maintain the same pose while looking at targets, and dynamic poses (MP) in which subjects perform additional important head movements while looking. From this data, we cropped around 80K images of the left and right eyes and frontalized them according to [13]. The labeled world gaze groundtruth was converted accordingly in the Headpose Coordinate System (HCS).

MPIIGaze. This dataset [10] contains 1500 left and right eye images of 15 subjects, which were recorded under various conditions in head pose or illuminations and contains people with glasses. The provided images are gray scale and approximately of size 36×60 pixels, and are already frontalized relying on the head pose yaw and pitch. The provide gaze is labeled in Headpose Coordinate System (HCS). Note that although in [10] the head pose was used as input for gaze

prediction, this did not improve our results in experiments so it was not used for the experiments reported below.

UT-Multiview. This dataset [19] comprises 23040 (1280 real and 21760 synthesized) left and right eye samples for each of the 50 subjects (15 female and 35 male). It was collected under laboratory condition, with various head poses. Eye images are gray scale and of size 36×60 pixels. They are not frontalized but accurate headpose and gaze in HCS are provided. Thus, in experiments, we concatenated the head pose in the network as described in [10]. More precisely, we concatenated the head pose $\mathbf{h}(I) \in R^{1 \times 2}$ of the input I image with the last fully-connected layers for the baseline CNN (Fig. 4), and did the same for the differential network, i.e. we concatenated the two head pose $\mathbf{h}(I)$ and $\mathbf{h}(J)$ of the input pair (I, J) with the last fully-connected layer in Fig. 6.

B. Experimental protocol

Cross-Validation. For the EYEDIAP and MPIIGaze datasets, we applied a leave-one-subject-out protocol, while due to its size, we used a 3-fold cross-validation protocol for the UT-Multiview dataset. Note that for this dataset, we train with real and synthesis data, but only test on real data. Note that the protocols for MPIIGaze and UT-Multiview are the ones from the original paper and followed by other researchers.

Performance measure. We trained and tested models for the left and right eyes separately, as we noticed that the left and right eyes may have different structures, and importantly, the labelled gaze might follow different distributions.

Following the above protocols, the error was defined as the average of the average gaze angular error computed for each fold, according to [10].

Selection of reference samples. For the linear adaptation and the differential NN methods, reference images are required to predict the gaze of the given subject. In these cases, unless stated otherwise, we randomly selected 9 points in the test set \mathcal{D}_{Test} for 200 times, and reported the average error computed for each random selection as defined above.

Tested models. Several methods were tested for comparison.

- **Baseline:** it corresponds to the generic model introduced in Section 2, and is our implementation of the neural

TABLE I: Average angular error (degree \pm STD) on three public datasets. ‘L, R, Avg’ denote the left, right eyes and the average of them. Note that the *Baseline* method does not require calibration data.

	EYEDIAP			MPIIGaze			UT-multiview		
	L	R	Avg	L	R	Avg	L	R	Avg
GazeNET [16]	-	-	-	-	-	5.5	-	-	4.4
<i>Baseline</i> [10]	5.37 ± 2.7	6.63 ± 2.8	6.00 ± 2.8	5.97 ± 1.2	6.25 ± 0.9	6.11 ± 1.1	6.08 ± 1.6	5.83 ± 1.6	5.95 ± 1.6
<i>SVR-Ad</i> [6]	4.14 ± 1.3	4.06 ± 1.2	4.10 ± 1.2	5.71 ± 1.3	5.78 ± 1.2	5.75 ± 1.3	5.61 ± 1.2	6.02 ± 0.8	5.82 ± 1.0
<i>Lin-Ad</i>	3.88 ± 1.6	3.81 ± 1.6	3.84 ± 1.6	5.68 ± 1.4	5.66 ± 1.3	5.67 ± 1.4	4.57 ± 0.1	4.56 ± 0.1	4.56 ± 0.1
<i>Diff-NN</i>	3.23 ± 1.3	3.23 ± 1.2	3.23 ± 1.3	4.69 ± 1.2	4.62 ± 1.1	4.64 ± 1.1	4.17 ± 1.2	4.08 ± 1.2	4.13 ± 1.1

network in [10], which achieves similar or better results than [10]. Note that [16] updates the result from [10] using a much deeper VGG-16 network. For real-time purpose, we use shallow networks, so we use our generic model as baseline for a fair comparison.

- **SVR-Ad** is our implementation of the SVR adaptation method of [6] built upon the *Baseline* model above. More precisely, following [6], the featuremap F2 (last layer before the output, see Fig. 4) is extracted as eye image features. A SVR model is trained using the reference image features and their gaze groundtruth, and then applied on the test eye image features for prediction.
- **Lin-Ad** corresponds to the *Baseline* model followed by linear adaptation (Section 2.2).
- **Diff-NN** is the method we propose, with the default parameters introduced in the paper.

C. Experimental results

The experimental results are presented in Table I.

Baseline model. First, let us note that under the same protocol, our *Baseline* model works slightly better than [10], which reported an error of 6.3° on MPIIGaze, and of 5.9° on UT-Multiview. This is probably due to our network architecture being slightly more complex, while still avoiding overfitting.

Linear and SVR Adaptation. Results demonstrate that, as expected, calibration helps and that our linear adaption method can greatly improve the baseline results, with an error decrease of (for the left and right eyes): 27.7% and 43.3% on EYEDIAP, 24.7% and 21.8% on UT-Multiview, and 4.9% and 9.4% on MPIIGaze. The difference in gain is most probably due to the recording protocols. While the EYEDIAP and UT-Multiview datasets were mainly recorded over the course of one session, the MPIIGaze dataset was collected in the wild, over a much longer period of time, and with much more lighting variability (but less head pose variability). This can be observed in Fig. 5 showing typical scattering plots of the EYEDIAP and MPIIGaze datasets. The EYEDIAP plots follow a more straight and compact linear relationship than those on the MPIIGaze dataset, reflecting the higher variability within the last dataset. Seen differently, we can interpret the results as having a session-based adaptation in the EYEDIAP

and UT-Multiview cases, whereas in MPIIGaze, the adaptation is more truly subject-based.

Results also show that our linear adaptation *Lin-Ad* method is working better than the *SVR-Ad* adaption approach [6], with an average gain of 6.3%, 1.4% and 21.5% on the EYEDIAP, MPIIGaze, and UT-Multiview datasets, respectively. The main reason might be that in *SVR-Ad*, the regression weights from the feature layer F2 are not exploited, in spite of their importance regarding gaze prediction. In addition, finding an appropriate kernel in the 256 dimensional space of F2 might not be so easy, and 9 points might not be sufficient for regression within such a space.

Differential method. Our approach *Diff-NN* performs much better than the other two adaptation methods which, on average over the 3 datasets, have an error 17.4% (*Lin-Ad*) and 30.6% (*SVR-Ad*) higher than ours. In particular, we can note that the gain is particularly important on the MPIIGaze dataset (22.2% compared to *Lin-Ad*), demonstrating that our strategy of directly predicting the gaze differences from pairs of images -hence allowing to implicitly match and compare these images- using our differential network is more powerful, and more robust against eye appearance variations across time, places, or illumination, than adaptation methods relying on gaze predictions only (*Lin-Ad*), or on compact eye image representations (*SVR-Ad*). On other more ‘session-based’ datasets, our linear adaptation method is already doing well, so that the gain is lower (around 10% on average).

D. Impact of reference samples

In this section, we discuss the impact of the reference samples on the results. We first analyse the variability associated to the choice of the related samples, and then study the number of samples required to achieve good results.

Calibration data variability. The performance of the adaptation methods are computed as the average over 200 random selection of 9 calibration samples. Depending on the selection (samples might be noisy, or not distributed well on the gaze grid), results may differ. Fig. 7 illustrates the variabilities of *Lin-Ad* and *Diff-NN* for the different trials of two subjects.

The example on the left shows a typical example where there is a relatively large bias for the given subject. In that case, whatever the selection of the calibration samples, the results of both *Lin-Ad* and *Diff-NN* are better than the baseline. The example on the right shows one of the few cases where the baseline is already good, with little bias but nevertheless quite noisy samples. In that case, there is only around 60% chances to obtain a better result with the linear adaptation, but still around 90% chances with our approach. Also, importantly, our *Diff-NN* approach is much less sensitive to the choice of calibration points than *Lin-Ad*, as can be seen from the higher and concentrated peaks in the error distributions.

Discussion about the selection of references. Fig. 7 shows the distribution of average angular errors due to the random selection of the reference images, which indicates that some of the selection work better than others. We can further analyse the impact of the reference samples on performance by measuring the error when using a single sample.

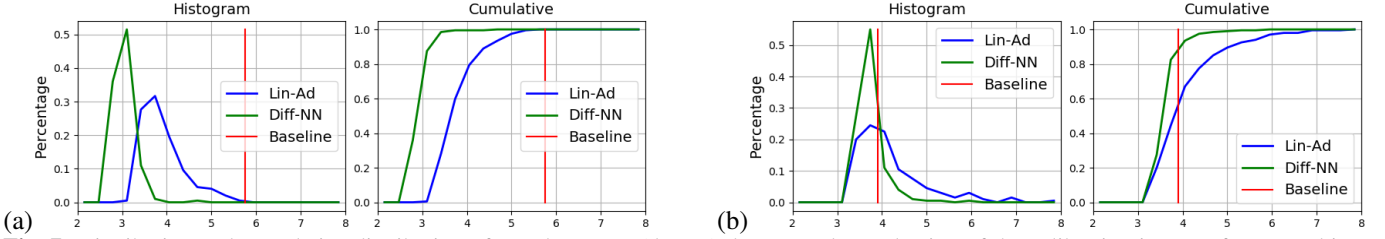


Fig. 7: Distribution and cumulative distribution of angular errors (degree) due to random selection of the calibration images, for two subjects (one from the MPIIGaze dataset, one from the EYEDIAP dataset), and for different methods: *Diff-NN* (green curve), *Lin-Ad* (blue curve), *Baseline* (red; note that this method does not rely on calibration data).

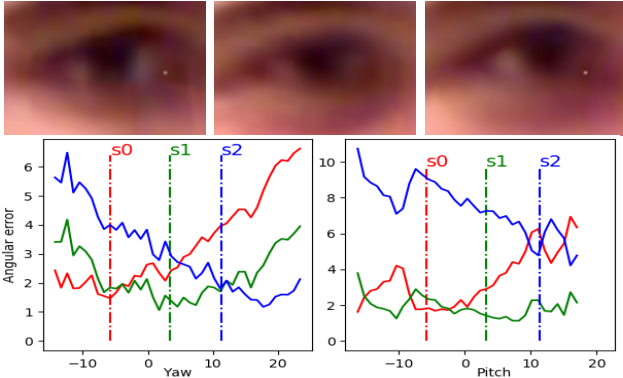


Fig. 8: The top row shows three different reference image, s_0 , s_1 , s_2 . The bottom row plots the average angular prediction error (degree) of samples in function of their absolute yaw (left plot) or pitch (right plot) when using a single reference sample s_0 (red curve), s_1 (green) and s_2 (blue) for prediction.

This is illustrated in Fig. 8, in which we selected three different images, denoted as s_0 , s_1 , s_2 , and used each one alone as reference to predict the gaze of this subject. The corresponding average errors (considering all other images of that subject) are shown as red, green and blue lines.

As expected, we can mainly observe that the prediction is more accurate when the test sample is closer to the reference sample, and vice versa. This is the main motivation of using weighted sum in Eq. (4). We can also notice that the error profiles are quite different, suggesting that better weighting scheme should be exploited. This is left for future work.

Discussion about the number of references. In Fig. 9 we also present adaptation results on the EYEDIAP dataset using different number of reference images.

When given few reference samples, the *SVR-Ad* and *Lin-Ad* underperform the *Baseline*, which is mainly due to the noise illustrated in Fig. 5, which introduce a high variability (and error) in the fitting process, especially for *Lin-Ad*. As the number of reference samples increases, the error of *Lin-Ad* decreases significantly because more accurate linear parameters can be obtained for adaptation. The error of *SVR-Ad* decreases more slowly at the beginning, but catches up that of *Lin-Ad* when using more samples, due to the inherent ability of *SVR-Ad* at leveraging more reference samples.

The *Diff-NN* outperforms the other methods even when using only one reference samples. This is not surprising because *Diff-NN* does not learn any model or parameter from the reference samples, but rather relies on richer information (the image context) to infer the difference rather than just the predicted gaze. Another interesting point is that, given

as many as 20 reference samples, there is still a noticeable margin between the results of *Diff-NN* and other methods.

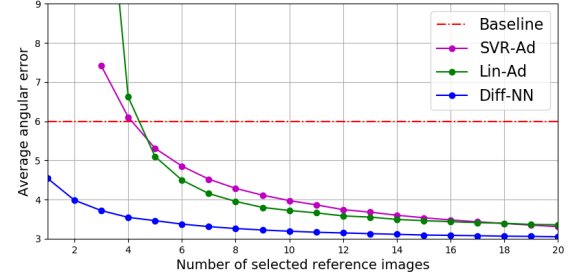


Fig. 9: Comparison of average angular error in degree (average of the left right eyes) for different methods in function of the number of reference images on EYEDIAP dataset. Note that the *Baseline* method does not require calibration data.

E. Reference weighting scheme

In this Section we analyse the weighting scheme combining the different predictions made from each reference image (see Eq. (4)), and more specifically, the influence of the Gaussian kernel bandwidth σ . Intuitively, when σ is too small, mainly the closest reference sample will contribute to the prediction. Conversely, when σ is too large, reference samples will have similar contributions.

Results are shown in Fig. 10. When σ varies from 5.7 to 22.8 degrees, the error stays low, changing in a narrow range of 0.1. It indicates that the *Diff-NN* is very robust w.r.t the weights. Similar results are also observed on MPIIGaze and UT-Multiview datasets.

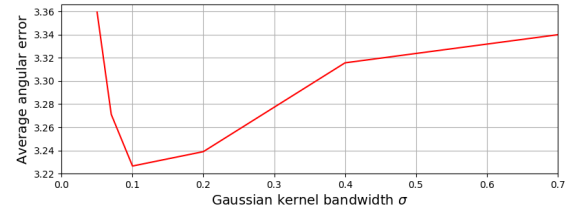


Fig. 10: Average angular error (degree) on EYEDIAP dataset with different Gaussian kernel bandwidth σ (in radian).

F. System design

Designing the network architecture and overall system can be motivated by several factors and principles. The main idea behind the differential network is that it can implicitly register and align images of the same eyes and from there better compute the (differential) elements (iris location, eye corners, eyelid closing) which really matters for gaze estimation than when abstracting these from a single image.

TABLE II: Average angular error (degree) on EYEDIAP dataset for different systems (see text).

Sys-1-early	Sys-2-proposed	Sys-3-late	Sys-4-siamese	Sys-5
3.40	3.23	3.47	3.40	3.76

We thus investigated different schemes and different levels at which to fuse the information coming from the two eye images. Early fusion can be achieved by concatenating the two eye images and using it as network input to the baseline architecture (See Fig. 4). It allows a direct comparison of the raw signals and fine geometric analysis, but also suffers from drawbacks: it may encounter difficulties in performing an implicit eye alignment if eyes are too far apart in the two images; abstracting important eye structures for gaze difference prediction might be difficult because the information coming from the two eyes is mixed in the layers; the complexity increases, as all image pairs (input, reference) need to be fully processed. At the other end, late fusion can be conducted by concatenating the F2 feature maps of the two images. The F2 eye representation might contain high level eye representations tuned to the prediction of differential gaze, but there might be a loss of localization information.

Our proposed network lies in between. It relies on intermediate representations of each eye allowing in principle the implicit registration of the two eyes from the processed images while extracting high level information relevant for differential gaze regression. To verify the intuition behind the proposed scheme, we compared the following systems:

- 1) **Sys-1 - early fusion:** concatenate the two images;
- 2) **Sys-2 - proposed :** concatenate the F1 feature maps;
- 3) **Sys-3 - late fusion:** concatenate the F2 feature map;
- 4) **Sys-4 - siamese:** two parallel *Baseline* networks with shared weights trained to only predict gaze differences.
- 5) **Sys-5 - multi-task with adaptation:** it corresponds to Sys-4 but trained to predict both the absolute gaze and the difference (as in [45] for head pose). The trained baseline network is further adapted using the *Lin-Ad* scheme.

Results are shown in Table II, and show that our architecture achieves the best results. Note that Sys-5 (approach of [45] followed by *Lin-Ad*) is worse than all other systems, demonstrating the advantage of predicting differential gaze over absolute gaze. The results of the Sys-1,3,4 are close but still outperformed by our system Sys-2, showing that intermediate fusion is better than early or late fusion. We believe this is due to the ability of the CNN network layers to do some filtering and alignment of the two images, while the fully-connected layers combine this information to infer gaze differences.

G. Algorithm complexity

The *Diff-NN* adaptation method does not have the same complexity as the others. Compared to the CNN *Baseline*, the linear adaptation only requires the computation of Eq.(2), which has negligible computational cost. Our *Diff-NN* approach, however, requires to predict the gaze differences between the test sample and N_c reference images. Fortunately, its complexity is not N_c times that of the *Baseline* thanks to our differential architecture (see Fig. 6). Indeed, first we can pre-compute and save the feature maps at the last convolutional

TABLE III: Run-times (in ms) between the *Baseline* and our *Diff-NN* method, using mini-batch (*Diff-NN* *) computation or not.

	CPU			GPU		
	<i>Baseline</i>	<i>Diff-NN</i>	<i>Diff-NN</i> *	<i>Baseline</i>	<i>Diff-NN</i>	<i>Diff-NN</i> *
Run-time	2.5	7.6	3.5	1.4	4.0	1.5

neural layer of all the reference images, so that the computation of one gaze difference requires mainly the forward pass of one image. Secondly, the feature maps of the test image also need to be computed only once, which can be achieved by stacking the feature maps of the reference images in a mini-batch, and compute all gaze differences in parallel.

Table III compares the running time (in ms) for the *Baseline* and the different *Diff-NN* options (and $N_c = 9$). They have been obtained by computing the average run-time of processing 5000 images. The CPU is an Intel(R) Core(TM) i7-5930K with 6 kernels and 3.50GHz per kernel. The GPU is an Nvidia Tesla K40. The program is written in Python and Pytorch. Note that as the Pytorch library will call multiple kernels for computation, the CPU-based run-time is also short. From this Table, we can see that our *Diff-NN* method and architecture has a computational complexity close to the *Baseline*.

H. Discussion

As can be seen, the method is working very well. We observe a gain for all datasets and users. Looking more carefully at results, we noticed the following. The yaw estimation is particularly good, while the pitch one is sometimes more problematic. This is illustrated in Fig. 8: when considering the *s2* reference sample, the estimated pitch is not very good on average (and even for *s0* and *s1*, the errors are larger on pitch than yaw). This behaviour is probably due to the following: when comparing two eye images, aligning laterally the two eyes relies on relatively stable structures (eye corners), and the iris horizontal location (related to the yaw) within the aligned eye can be estimated quite reliably, as it is given by strong vertical edges. However, visually, pitch estimation is much harder: the vertical alignment relies on eyelid contours, which are moving structures (correlated with the pitch, but only partially), and thus less stable across eye images, and since for common cases the top and bottom parts of the iris are hidden, the iris vertical position needs to be estimated from the shape of the iris vertical sides (see eyes in Fig. 8).

VI. CONCLUSION

This paper aims to improve appearance-based gaze estimation using subject specific models built from few calibration images. Our main contributions are to propose (1) a linear adaptation method based on these reference images; (2) a differential NN for predicting gaze differences instead of gaze directions to alleviate the impact of annoyance factors like illumination, cropping variability, variabilities in eye shapes. Experimental results on three public and commonly used datasets prove the efficacy of the proposed methods. More precisely, while the linear adaptation method can already boost the results on single session like situations, the differential NN method produces even more robust and stable results across different sessions of the same user, but costs some more run-time compared to a baseline CNN.

REFERENCES

- [1] S. Andrist, X. Z. Tan, M. Gleicher, and B. Mutlu, “Conversational gaze aversion for humanlike robots,” in *ACM/IEEE International Conference on Human-robot Interaction*, HRI ’14, (New York, NY, USA), pp. 25–32, ACM, 2014.
- [2] A. Moon, D. M. Troniak, B. Gleeson, M. K. Pan, M. Zheng, B. A. Blumer, K. MacLean, and E. A. Croft, “Meet me where i’m gazing: How shared attention gaze affects human-robot handover timing,” in *ACM/IEEE International Conference on Human-robot Interaction*, HRI ’14, (New York, NY, USA), pp. 334–341, ACM, 2014.
- [3] T. Pfeiffer, “Towards gaze interaction in immersive virtual reality: Evaluation of a monocular eye tracking set-up,” in *Virtuelle und Erweiterter Realität-Fünfter Workshop der GI-Fachgruppe VR/AR*, 2008.
- [4] R. Ishii, K. Otsuka, S. Kumano, and J. Yamato, “Prediction of who will be the next speaker and when using gaze behavior in multiparty meetings,” *ACM Transactions on Interactive Intelligent Systems*, vol. 6, pp. 4:1–4:31, May 2016.
- [5] M. Vidal, J. Turner, A. Bulling, and H. Gellersen, “Wearable eye tracking for mental health monitoring,” *Computer Communications*, vol. 35, no. 11, pp. 1306–1311, 2012.
- [6] K. Krafcik, A. Khosla, P. Kellnhofer, and H. Kannan, “Eye Tracking for Everyone,” *IEEE Conference on Computer Vision and Pattern Recognition*, pp. 2176–2184, 2016.
- [7] M. Tonsen, J. Steil, Y. Sugano, and A. Bulling, “Invisibleeye: Mobile eye tracking using multiple low-resolution cameras and learning-based gaze estimation,” *ACM on Interactive, Mobile, Wearable and Ubiquitous Technologies*, vol. 1, no. 3, 2017.
- [8] Q. Huang, A. Veeraraghavan, and A. Sabharwal, “Tabletgaze: unconstrained appearance-based gaze estimation in mobile tablets,” *arXiv preprint arXiv:1508.01244*, 2015.
- [9] D. W. Hansen and Q. Ji, “In the eye of the beholder: A survey of models for eyes and gaze,” *IEEE transactions on pattern analysis and machine intelligence*, vol. 32, no. 3, pp. 478–500, 2010.
- [10] X. Zhang, Y. Sugano, M. Fritz, and A. Bulling, “Appearance-based gaze estimation in the wild,” in *IEEE Conference on Computer Vision and Pattern Recognition*, pp. 4511–4520, IEEE, jun 2015.
- [11] Y. Sugano, Y. Matsushita, and Y. Sato, “Learning-by-synthesis for appearance-based 3D gaze estimation,” *Proceedings of the IEEE Computer Society Conference on Computer Vision and Pattern Recognition*, pp. 1821–1828, 2014.
- [12] W. Zhu and H. Deng, “Monocular free-head 3d gaze tracking with deep learning and geometry constraints,” in *The IEEE International Conference on Computer Vision*, Oct 2017.
- [13] K. A. Funes Mora and J.-M. Odobez, “Gaze estimation in the 3d space using rgb-d sensors,” *International Journal of Computer Vision*, vol. 118, no. 2, pp. 194–216, 2016.
- [14] A. Shrivastava, T. Pfister, O. Tuzel, J. Susskind, W. Wang, and R. Webb, “Learning from simulated and unsupervised images through adversarial training,” in *IEEE Conference on Computer Vision and Pattern Recognition*, pp. 2107–2116, 2017.
- [15] C. Zhang, R. Yao, and J. Cai, “Efficient eye typing with 9-direction gaze estimation,” *Multimedia Tools and Applications*, pp. 1–18, 2017.
- [16] X. Zhang, Y. Sugano, M. Fritz, and A. Bulling, “It’s written all over your face: Full-face appearance-based gaze estimation,” in *IEEE International Conference on Computer Vision and Pattern Recognition Workshops*, 2017.
- [17] E. D. Guestrin and M. Eizenman, “General theory of remote gaze estimation using the pupil center and corneal reflections,” *IEEE Transactions on biomedical engineering*, vol. 53, no. 6, pp. 1124–1133, 2006.
- [18] K. A. Funes Mora and J.-M. Odobez, “Geometric Generative Gaze Estimation (G 3 E) for Remote RGB-D Cameras,” pp. 1773–1780, jun 2014.
- [19] Y. Sugano, Y. Matsushita, and Y. Sato, “Learning-by-synthesis for appearance-based 3d gaze estimation,” in *IEEE Conference on Computer Vision and Pattern Recognition*, pp. 1821–1828, IEEE, 2014.
- [20] Z. Tósér, R. A. Rill, K. Faragó, L. A. Jeni, and A. Lőrincz, “Personalization of gaze direction estimation with deep learning,” in *Joint German/Austrian Conference on Artificial Intelligence (Künstliche Intelligenz)*, pp. 200–207, Springer, 2016.
- [21] D. Masko, *Calibration in Eye Tracking Using Transfer Learning*. PhD thesis, KTH ROYAL INSTITUTE OF TECHNOLOGY, 2017.
- [22] F. Lu, Y. Sugano, T. Okabe, and Y. Sato, “Adaptive Linear Regression for Appearance-Based Gaze Estimation,” *Pami*, vol. 36, no. 10, pp. 2033–2046, 2014.
- [23] K. A. Funes Mora, F. Monay, and J.-M. Odobez, “Eyediap: A database for the development and evaluation of gaze estimation algorithms from rgb and rgb-d cameras,” in *Proceedings of the Symposium on Eye Tracking Research and Applications*, pp. 255–258, ACM, 2014.
- [24] G. Liu, Y. Yu, K. A. Funes-Mora, and J.-M. Odobez, “A differential approach for gaze estimation with calibration,” in *The British Machine Vision Conference*, The British Machine Vision Association, 2018.
- [25] E. Wood and A. Bulling, “Eyetab: Model-based gaze estimation on unmodified tablet computers,” *ACM Symposium on Eye Tracking Research and Applications*, pp. 3–6, 2014.
- [26] K. A. Mora Funes and J.-M. Odobez, “3D Gaze Tracking and Automatic Gaze Coding from RGB-D Cameras,” *IEEE Conference in Computer Vision and Pattern Recognition, Vision Meets Cognition Workshop*, pp. 4321–4322, 2014.
- [27] R. Valenti, N. Sebe, and T. Gevers, “Combining head pose and eye location information for gaze estimation,” *IEEE Transactions on Image Processing*, vol. 21, no. 2, pp. 802–815, 2012.
- [28] L. Sun, M. Song, Z. Liu, and M.-T. Sun, “Real-time gaze estimation with online calibration,” *IEEE MultiMedia*, vol. 21, no. 4, pp. 28–37, 2014.
- [29] E. Wood, T. Baltrušaitis, L.-P. Morency, P. Robinson, and A. Bulling, “A 3d morphable eye region model for gaze estimation,” in *European Conference on Computer Vision*, pp. 297–313, Springer, 2016.
- [30] K. Wang and Q. Ji, “Real Time Eye Gaze Tracking with Kinect,” *IEEE conference on Computer Vision*, pp. 1003–1011, 2017.
- [31] K. Simonyan and A. Zisserman, “Very deep convolutional networks for large-scale image recognition,” *arXiv preprint arXiv:1409.1556*, 2014.
- [32] X. Zhang, Y. Sugano, M. Fritz, and A. Bulling, “MPIIGaze: Real-World Dataset and Deep Appearance-Based Gaze Estimation,” *IEEE Transactions on Pattern Analysis and Machine Intelligence*, pp. 1–14, 2017.
- [33] A. Lanata, G. Valenza, A. Greco, and E. P. Scilingo, “Robust head mounted wearable eye tracking system for dynamical calibration,” *Journal of Eye Movement Research*, vol. 8, no. 5, 2015.
- [34] M. Mansouriyan, J. Steil, Y. Sugano, and A. Bulling, “3d gaze estimation from 2d pupil positions on monocular head-mounted eye trackers,” in *Proceedings of the Ninth Biennial ACM Symposium on Eye Tracking Research & Applications*, pp. 197–200, ACM, 2016.
- [35] Y. Sugano and A. Bulling, “Self-calibrating head-mounted eye trackers using egocentric visual saliency,” in *Proceedings of the 28th Annual ACM Symposium on User Interface Software & Technology*, pp. 363–372, ACM, 2015.
- [36] X. Zhang, M. X. Huang, Y. Sugano, and A. Bulling, “Training person-specific gaze estimators from user interactions with multiple devices,” in *Proceedings of the 2018 CHI Conference on Human Factors in Computing Systems*, p. 624, ACM, 2018.
- [37] J. Bromley, I. Guyon, Y. LeCun, E. Säckinger, and R. Shah, “Signature verification using a “siamese” time delay neural network,” in *Advances in Neural Information Processing Systems*, pp. 737–744, 1994.
- [38] S. Zagoruyko and N. Komodakis, “Learning to compare image patches via convolutional neural networks,” in *IEEE Conference on Computer Vision and Pattern Recognition*, pp. 4353–4361, IEEE, 2015.
- [39] E. Simo-Serra, E. Trulls, L. Ferraz, I. Kokkinos, P. Fua, and F. Moreno-Noguer, “Discriminative learning of deep convolutional feature point descriptors,” in *IEEE International Conference on Computer Vision*, pp. 118–126, IEEE, 2015.
- [40] B. G. Kumar, G. Carneiro, I. Reid, et al., “Learning local image descriptors with deep siamese and triplet convolutional networks by minimising global loss functions,” in *IEEE Conference on Computer Vision and Pattern Recognition*, pp. 5385–5394, 2016.
- [41] F. Wang, L. Kang, and Y. Li, “Sketch-based 3d shape retrieval using convolutional neural networks,” in *IEEE Conference on Computer Vision and Pattern Recognition*, pp. 1875–1883, IEEE, 2015.
- [42] W. Luo, A. G. Schwing, and R. Urtasun, “Efficient deep learning for stereo matching,” in *IEEE Conference on Computer Vision and Pattern Recognition*, pp. 5695–5703, 2016.
- [43] N. McLaughlin, J. M. del Rincon, and P. Miller, “Recurrent convolutional network for video-based person re-identification,” in *IEEE Conference on Computer Vision and Pattern Recognition*, pp. 1325–1334, IEEE, 2016.
- [44] R. R. Varior, M. Haloi, and G. Wang, “Gated siamese convolutional neural network architecture for human re-identification,” in *European Conference on Computer Vision*, pp. 791–808, Springer, 2016.
- [45] M. Venturelli, G. Borghi, R. Vezzani, and R. Cucchiara, “From depth data to head pose estimation: a siamese approach,” *arXiv preprint arXiv:1703.03624*, 2017.